3DVAR Retrieval of 3D Moisture Field from Slant-path Water Vapor Observations of a High-resolution Hypothetical GPS Network

Haixia Liu and Ming Xue*

School of Meteorology and Center for Analysis and Prediction of Storms University of Oklahoma, Norman OK 73019

Submitted to Monthly Weather Review

August 2004

*Corresponding Author Address:
Dr. Ming Xue
School of Meteorology
University of Oklahoma
100 E. Boyd
Norman OK 73019
mxue@ou.edu

Abstract

A new 3DVAR method is developed to retrieve three-dimensional moisture field of atmosphere from a ground-based GPS slant-path water vapor (SWV) observation network. In this method, the inclusion of an analysis background makes the retrieval feasible. An explicit Gaussian spatial filter is used to model the background error covariances. Anisotropic spatial filter that is based on flow-dependent background error structures is implemented and tested. The anisotropic filter coefficients are derived from true background error field or from the error in an intermediate analysis obtained using an isotropic filter. In the latter case, an iterative procedure is involved.

A set of observing system simulation experiments is conducted to test the new method with a dryline case that occurred during IHOP 2002. Results illustrate that this system can properly recover three-dimensional mesoscale moisture structures from GPS SWV data and surface moisture observations. The analysis captures major features in the water vapor field associated with the dryline, even when an isotropic spatial filter is used. The use of flow-dependent background error covariance modeled by the anisotropic spatial filter further improves the moisture retrieval.

Sensitivity tests show that surface moisture observations are important for the analysis near ground, especially when flow-dependent background error covariances are not used. Vertical filtering is necessary for obtaining accurate analysis increment at the low levels. Retrieved moisture field with this new method is not very sensitive to the errors in the surface moisture observations and GPS SWV data. The role of flow-dependent background error covariance is more prominent when the density of ground-based GPS receiver stations decreases.

1. Introduction

It is very important to accurately characterize the three-dimensional distribution of water vapor in the atmosphere for the understanding and prediction of mesoscale and storm-scale weather, especially with regard to quantitative precipitation forecasting (Emanuel *et al.* 1995). Skills in quantitative precipitation forecasting have been improved rather slowly owing to the high spatial and temporal variability of water vapor. Thus, high-resolution observations of three-dimensional water vapor should have potential to significantly improve the prediction of precipitation and severe weather.

Existing measurement methods of 3D water vapor field include mainly radiosonde, ground- and space-based water vapor radiometers. Radiosonde measurements carry significant operational costs and neither its spatial or temporal resolution is not good enough to capture water vapor variations. Under severe weather conditions, the poor performance of radiosonde moisture sensors currently in use prevents effective use of these measurements. The radiometers cannot satisfy our needs for measuring water vapor variation in atmosphere, either. They do not function well under all weather conditions even though they are capable of global coverage and overcome the temporal resolution problem. In recent years, spaced- and ground-based Global Positioning Systems (GPS) have been developed and become an important instrument that can potentially provide water vapor measurements with high resolution under virtually all weather conditions (Businger *et al.* 1996; Ware *et al.* 2000; Wolfe and Gutman 2000; Bengtsson *et al.* 2003).

The microwave radio signals transmitted by GPS satellites are delayed by the atmosphere as they propagate to the ground-based GPS receivers. The total delay along the slant path is composed of three parts: ionospheric delay, hydrostatic delay and wet delay. Ionospheric delay

observed by a dual-frequency GPS receiver can be calculated to millimeter accuracy. The hydrostatic delay can be estimated with known knowledge of pressure and temperature. So the slant-path wet delay (SWD) is obtained by subtracting the ionospheric and hydrostatic delays from the total delay. Then zenith wet delay (ZWD) can be obtained by projecting SWD observations onto the zenith and averaging them over a certain time period. Further, the precipitable water (PW, defined as the vertically integrated water vapor) can be calculated from ZWD (Bevis *et al.* 1994; Duan *et al.* 1996). In recent years, researchers have demonstrated that assimilating observations of ZWD and PW data into mesoscale numerical models provides beneficial impacts on short-range precipitation forecast of convective weather (Kuo *et al.* 1993; Kuo *et al.* 1996; Guo *et al.* 2000; Falvey and Beavan 2002). Further, Ha et al (2003) showed that the assimilation of SWD is superior to that of PW both in recovering water vapor information and in short-range precipitation forecast.

De Pondeca and Zou (2001a) assimilated simulated GPS observations, called zenith total delay (ZTD), which is made up of zenith hydrostatic delay (ZHD) and ZWD into a mesoscale model and showed that the vertically integrated moisture was very accurately verified against the observations and an overall improvement was achieved in the retrieved vertical profiles of the moisture fields. Further, they (de Pondeca and Zou 2001b) performed a case study of the passage of a winter frontal system with variational assimilation of ZTD. The work further verified that the assimilation of GPS ZTD observations has a positive impact on the model prediction.

In addition to the four-dimensional variational (4DVAR) assimilation method that is used in some of the afore-quoted work, the three-dimensional variational (3DVAR) method has also been used. Such work includes Cucurull et al (2004) who assimilated ground-based GPS ZTD

data for a storm event over the western Mediterranean Sea, and MacDonald et al (2002) who tested a 3DVAR procedure with slant-path water vapor data from a mesoscale hypothetical GPS ground receiver network to recover three-dimensional atmospheric moisture field. Since ZTD, ZWD and PW only give the vertically integrated measurements which do not provide information about the vertical structure of the atmosphere directly, variational techniques that solve a global minimization problem is a nature choice for analyzing such data. A variational method produces a solution that gives the best fit of the analyzed integrated total water vapor to observations, subjecting to the background constraint. Further, variational methods are also more suitable in directly assimilating indirect observations, i.e., observations that are not the analysis variables themselves.

ZTD, ZWD and PW data are products derived from the original total delay along the slant paths of GPS observations. The derivation involves additional assumptions. With variational method available as a powerful analysis tool, it is better to directly use the GPS slant-path observations to obtain a three-dimensional moisture distribution. Therefore, the slant-path water vapor observation is the focus of this paper. Similar to the relationship of ZWD and PW, since the SWD is nearly proportional to the quantity of water vapor integrated along the slant path, the relationship between the SWD and SWV is (Bevis *et al.* 1994),

$$SWV = \Pi \bullet SWD, \tag{1}$$

where SWV and SWD are given in units of length, and Π is a dimensionless constant, a function of weighted mean temperature of the atmosphere. The accuracy of SWV with this method is about a few millimeters (Ware et al. 1997; Braun et al. 2001). Most importantly, SWV can provide vertical structure information of atmospheric moisture distribution through intercepting paths. MacDonald et al (2002) demonstrates through Observing System Simulation Experiments

(OSSE) and 3DVAR analysis that a high-resolution network of GPS receivers can recover the moisture field from the slant integrated water vapor. In their analysis, the integrated slant water vapor measurements are combined with the surface moisture observations assumed to be available at each ground station and with a low-density network of water vapor soundings.

In this paper, we follow the standard practice of 3DVAR data assimilation for NWP (Lorenc 1981; Daley 1991) by including the analysis background. Consequently, the cost function includes both background and observation constraint terms. A non-negative-moisture weak constraint is also included in this cost function. The use of a background makes the problem over-determined and the retrieval feasible for experiments in which only 9 GPS satellites are simultaneously in view per ground-based receiver. Furthermore, proper spread of observation in space is achieved in our analysis through background error correlation. In this study, a Gaussian spatial filter is used to model background error covariance, and the implementation allows for flow-dependent anisotropic filtering. Unlike the multi-grid approach used in (MacDonald *et al.* 2002), filtering based on background error makes it easy to control or assess the amount of spatial smoothing being applied, which affects the weighting and spread of observational information therefore the quality of analysis.

We report in the following our work to analyze 3D water vapor distribution from a hypothetical GPS observation network. Section 2 introduces our 3DVAR analysis system. Section 3 describes the generation of a simulated GPS SWV data set using the Advanced Regional Prediction System (ARPS). Retrieval experiments and numerical results will be presented in Section 4. Further discussions on the use of this method are given in Section 5 through sensitivity experiments. Conclusions and an outline of future work are given in the final section.

2. 3DVAR Retrieval Method

The retrieval method used in this paper is based on 3DVAR method (Lorenc 1981; Daley 1991) of data assimilation which is to minimize the following cost function,

$$J(x) = J_{b}(x) + J_{swv}(x) + J_{sfc}(x) + J_{c}(x)$$

$$= \frac{1}{2} (x - x_{b})^{T} \mathbf{B}^{-1} (x - x_{b}) + \frac{1}{2} \left[H_{swv}(x) - SWV \right]^{T} \mathbf{R}_{swv}^{-1} \left[H_{swv}(x) - SWV \right]$$

$$+ \frac{1}{2} \left[H_{sfc}(x) - q_{v_{sfc}} \right]^{T} \mathbf{R}_{sfc}^{-1} \left[H_{sfc}(x) - q_{v_{sfc}} \right] + \frac{1}{2} \left(\frac{|x| - x}{2} \right)^{2}$$
(2)

where the cost function J is composed of four terms: background constraint term, GPS SWV observation term, the term for conventional surface moisture observations and the non-negative weak constraint. The x, often a vector, is the control variable which in our case contains the specific humidity q_v at every grid point. x_b is the corresponding background state vector. The first term, J_b , represents the departure of the control variable from the background. **B** is the background error covariance matrix, which decides how the observation information is spread as well as weighted (in combination with the observation errors) in the analysis domain.

The second term, J_{swv} , represents the departure of the analysis, calculated from control variable q_v through the observation operator H_{swv} , from the observations SWV that is measured by the ground-based GPS network. The matrix \mathbf{R}_{swv} is the observation error covariance matrix, which is often simplified to be diagonal under the assumption that observation errors are not correlated. The magnitude of variances, the diagonal elements of matrix \mathbf{R}_{swv} , compared to the background error variances, determines the relative weight of observation and background for the analysis. In our paper, observation error variances for SWV and surface observations are specified whose values are given later.

Since the ground-based GPS receiver sites are commonly equipped with regular meteorological sensors, the regular surface water vapor observations can be available together

with SWV observations. As a consequence, J_{sfc} , is added in the cost function to better recover the moisture structure near surface. Finally, in order to avoid the negative water vapor at high levels in the minimization process, a non-negative-moisture weak constraint term, J_c , is also included in this cost function.

As pointed out previously, the inclusion of background term is significant for the 3DVAR analysis. It not only can eliminate the under-determined problem associated with the number of control variables exceeding the number of observations, but also provide more accurate analysis through the background error covariance matrix. But since **B** is very large for typical meteorological problems, its direct inversion as required by (2) is therefore never attempted. Huang (2000) presents a method named variational analysis using a filter (VAF), in which the control variable is redefined as,

$$v = \mathbf{B}^{-1} (x - x_b). \tag{3}$$

It is not the full analysis field itself but the increment field relative to the background, multiplied by the inverse of **B**. As a consequence, the cost function is redefined as,

$$J(v) = J_{b}(v) + J_{swv}(v) + J_{sfc}(v) + J_{c}(v)$$

$$= \frac{1}{2}v^{\mathsf{T}}\mathbf{B}^{\mathsf{T}}v + \frac{1}{2}\left[H_{swv}(\mathbf{B}v + x^{b}) - SWV\right]^{\mathsf{T}}\mathbf{R}_{swv}^{-1}\left[H_{swv}(\mathbf{B}v + x^{b}) - SWV\right]$$

$$+ \frac{1}{2}\left[H_{sfc}(\mathbf{B}v + x^{b}) - q_{v_{sfc}}\right]^{\mathsf{T}}\mathbf{R}_{sfc}^{-1}\left[H_{sfc}(\mathbf{B}v + x^{b}) - q_{v_{sfc}}\right]$$

$$+ \frac{1}{2}\left(\frac{|\mathbf{B}v + x^{b}| - (\mathbf{B}v + x^{b})}{2}\right)^{2}.$$

$$(4)$$

This modification avoids the inversion of **B** in the new cost function. Moreover, VAF method uses a spatial filter to model the effect of **B** matrix instead of calculating and storing the matrix. The new variational analysis scheme is simpler and more flexible in practical implementations. The choice of spatial filter should be based on a priori knowledge of the covariance matrix **B**.

For instance, the following Gaussian filter function can be used to represent **B** for homogeneous and isotropic background error field (Daley 1991) for a three-dimensional univariate problem,

$$b_{ij} = \sigma_b^2 \exp\left[-\left(\frac{r_{ij}}{L_r}\right)^2\right],\tag{5}$$

where σ_b^2 is the variance of background error, r_{ij} is the spatial distance between grid point i and grid point j, and L, is the length scale decided by the background error correlation and is in practical use sometimes tied to the observation station density. This model represents an isotropic background error covariance. It should be pointed out that a truncated Gaussian filter will be used in this paper to save memory. The truncation destroys the positiveness of the modified \mathbf{B} , so the Lanczos window (Duchon 1979) is chosen to improve iteration convergence. Previous work (Hayden and Purser 1995) has demonstrated that a recursive filter without the need of extra memory can asymptotically approach a Gaussian filter as the iteration goes to infinity. But Gaussian filter is simpler and much easier to model anisotropic covariances though more expensive than recursive filter. Additional details about the VAF method can be found in Huang (2000) and our 3DVAR analysis will be constructed based on this method.

The use of isotropic background error covariance is based on the assumption that background errors at nearby points are similar (Riishojgaard 1998). But the background error covariance should be flow-dependent and such covariance should improve the analysis, especially when data are sparse. Therefore, an anisotropic filter is considered to model the flow-dependent **B** matrix. Simply, the following expression can provide such an anisotropic filter,

$$b_{ij} = \sigma_b^2 \exp \left[-\left(\frac{r_{ij}}{L_r}\right)^2 \right] \exp \left[-\left(\frac{f_i - f_j}{L_f}\right)^2 \right]$$
 (6)

where f is a field whose pattern represents that of the background error and we will call it the error field. In this study, f is either the true error of the background or an estimate of it. L_f is the length scale in error field space, compared to the length scale L_r in physical space, and is decided by the correlation of background error. The new background error covariance between two points defined by the Eq. (6) will follow the shape of the error field and fall off rapidly in the directions where the error field gradient is strong while isotropic covariance will dominate in directions where the error field changes slowly. Eq. (6) shows that in the case L_f goes to infinity, the anisotropic covariance reduces to the isotropic form in Eq. (5).

The isotropic and anisotropic filters will be used respectively to model the behavior of the background error covariance and their analysis results will be compared to show how the flow-dependent background error covariance provide better analysis than the isotropic one does.

3. Observing System Simulation Experiment (OSSE)

Currently, high-resolution GPS observation network with large spatial coverage does not exist in the United States. We test our analysis system by using simulated data. Experiments as such as commonly referred as Observing System Simulation Experiments (OSSE) and are often used to test the performance of future observing systems. The model used to produce the simulated data set is the Advanced Regional Prediction System (ARPS, Xue *et al.* 2000) which is a nonhydrostatic model in a generalized terrain-following coordinate. High-resolution observations from hypothetical GPS networks are created from forecast fields for a dryline case that occurred on June19, 2002 over the Southern Great Plains during the CAPS IHOP real-time forecast period (Xue *et al.* 2002). The ARPS model is initialized using analysis of the ARPS Data Analysis System (ADAS, Brewster 1996) at 1200 UTC June 19, 2002, and integrated for 8

hours. The computational domain is over the Southern Great Plains with 9 km grid spacing and 43 layers in the vertical. Stretched vertical grid coordinate is used with a minimum vertical grid spacing of 100 meters in boundary layer.

Considering that in the near future, mean spacing of ground receivers of GPS observation networks will probably not be much less than a hundred kilometers, thus the scale of water vapor distribution we can obtain should be of mesoscale. The 9-km 8-hour forecast field, therefore, is thinned by sampling specific humidity every 4 grid points, yielding a resolution of 36 km and a horizontal grid size of 46×41. This gridded field is defined as the 'nature' and used to generate the hypothetical GPS slant water vapor observation data. The specific humidity field from the 'nature' is presented in Fig. 1. A roughly north-south zone of sharp horizontal moisture gradient is located to the west of Kansas, Oklahoma and Texas, corresponding to a dryline located in the region (Fig. 1a). The east-west vertical slice at y=234 km (Fig. 1b) shows that a vertically oriented boundary between dry and wet air is found in the lowest 1.5 km and becomes nearly horizontal off to the east. The upward bulging moisture tongue near x = 576 km reflects upward motion occurring there. To the west of the dryline, the atmosphere is well-mixed up to 500mb. Such strong gradient as well as the variations in strong gradient in water vapor may not be properly captured by ordinary moisture observation networks, especially at levels away from the ground. However, the integrated water vapor along slant paths between surface GPS receivers and satellites can provide three-dimensional information with high temporal and spatial resolutions.

For our OSS experiments, the slant-path water vapor is obtained by formula,

$$SWV_{ij} = \int_{i^{th} receiver}^{jth satellite} q_{v} ds, \tag{7}$$

where ds is the length of elements along slant path, SWV_{ij} the integrated water vapor along the slant path between the i^{th} ground-based GPS receiver and the j^{th} GPS satellite, and q_v is the specific humidity along the path elements. This value is given by tri-linear interpolations from eight surrounding grid points. The hypothetical GPS network is composed of nine irregularly distributed satellites simultaneously in view, and of 132 ground-based receivers which are evenly distributed in the analysis domain. The horizontal resolution of GPS receivers is 144 km. Both sampling and analysis grids are on the ARPS terrain-following coordinate. A schematic is given in Fig. 2 to illustrate the hypothetical GPS observation network. Surface moisture observations are available at GPS receiver sites.

4. Retrieval experiments and results

a. Single surface observation test

Isotropic and anisotropic filters, defined respectively by Eqs. (5) and (6), are used to model background error covariance which plays a significant role in our retrieval system. In order to validate our newly developed system and understand the behaviors of the isotropic and anisotropic spatial filters, we first show in Fig. 3 the analysis increment field from a single specific humidity observation test using isotropic and anisotropic covariance models, respectively. For the former, the spatial correlation of background error is expressed by the function in Eq. (5). For the latter, the anisotropic covariance is modeled by the function in Eq. (6). L_r in anisotropic filter should be larger than that in isotropic filter so that the background error covariance shape is able to follow the error field. Its actual value is given below.

In this case, the observation vector q_{vsfc} in Eq. (4) consists of only one water vapor observation located at grid point (13, 18, 1) with a specific humidity value of 8.3 g kg⁻¹. This

observation station is marked by a black dot in Fig. 3. No SWV observation is involved in this test so that the second term in cost function disappears. The observation operator H_{sfc} can be ignored here (it has not effect) since the observation station is co-located with grid point and observation variable is the control variable itself. For simplicity, only two-dimensional horizontal filter is used so that the analysis is essentially two dimensional in this example. In the isotropic filter case, a horizontal length scale (L_r) of 4 grid intervals is used. In the anisotrophic filter case, L_r is given a 6 grid-interval length and the length scale in error field space $L_f = 2.0$ g kg⁻¹.

For the single observation tests, the error field *f* is chosen as the specific humidity field of the 'nature'. The background used in this case is horizontally homogeneous therefore the pattern of 'nature' field presents correctly the pattern of background error. The background specific humidity is 12.1 g kg⁻¹ at the surface. The observation information located at one grid point is spatially spread through the background error covariance (Fig. 3). The analysis increment for the single observation is determined by the structure of background error, consequently, the analysis with isotropic covariance gives a analysis increment of circular shape and that with anisotropic covariance exhibits an analysis increment that is clearly related to the specific humidity or the error field (Fig. 1a). The analysis increment pattern is oriented in NNE to SSW direction and is narrower in the east-west and broader in the north-south directions, respectively, compared to the circular increment of isotropic analysis. This structure is in accordance with the shape of the error field.

b. SWV retrieval experiments

The single observation tests show us the behaviors of isotropic and anisotropic filters for modeling the background error covariance. This analysis system is applied to the retrieval of

three-dimensional moisture from simulated GPS slant-path water vapor and surface moisture observations here. A list of retrieval experiments is given in Table 1. The overall correlation coefficients between analysis increment field for these experiments and the 'truth' increment field are also given in the table for these experiments.

First, a control experiment (CNTL) is performed. In this experiment, both SWV observations from the hypothetical GPS network and the regular surface moisture observations at the ground-based GPS receivers are used. The analysis background is created by smoothing the 'nature' field 50 times, using a 9-point filter in the horizontal. It can be seen from Fig. 4 that this background shows a general pattern of higher moisture to the east and lower values to the west. Detailed dryline structure is lost. Since both the truth and background are known, the background error can be calculated. It is therefore possible to model the background error covariance by taking the known background error as variable f in Eq. (6) and this is done for CNTL. The length scale L_r used is equal to 4 grid intervals in both horizontal and vertical directions. L_f is given as 2 g kg⁻¹. Owing to the insignificant effect of filter on the far distance, cutoff radii are used and chosen to be 10-grid intervals in the horizontal and 6 layers in the vertical, respectively. The selection of filter scale depends, for one thing, on the density of ground-based GPS receivers. The relatively small filter scales and cutoff radii are chosen here so that gaps between receiver stations are filled without excessive smoothing to the analysis. The relative weights of background, GPS SWV observations, regular surface moisture observations and non-negative weak constraint are specified as 1, 100, 500 and 50, respectively. The cost function defined by Eq. (4) is minimized with respect to the increment of specific humidity, using a conjugate gradient algorithm.

With above parameter settings, the control experiment is conducted. Figure 5 presents a vertical cross-section of retrieved moisture field at y = 234 km from this experiment. Only the vertical structure below 6 km is shown here since water vapor has very low values above 6 km. It is obvious that this retrieved moisture field matches the 'nature' very well. The dryline near x = 290 km is accurately captured. There is a strong east-west moisture gradient at the low levels and the moisture isohumes are almost perpendicular to the ground near the dryline. Meanwhile, due to presumably upward motion near the dryline at near x = 576 km, there exists one moisture tongue and two troughs to the east and west of the tongue, the latter due to return flows. Figure 6 shows the specific humidity increment at the surface. Retrieved increment matches almost exactly the increment of 'truth' (the difference of the truth from background); for instance, their shapes match and extremum locations coincide. The correlation coefficient of increment fields of between retrieval and 'truth' for the entire grid is about 0.926.

To see the performance of analysis when an isotropic filter is used, experiment, named SNF, is conducted. It is the same as CNTL except that the filter is independent of the flow and is isotropic. The length scale for isotropic filter should be smaller than that for anisotropic filter, so the L_r in this test is given as 3-grid intervals. Figure 7 shows the vertical cross-section at y = 234 km and analysis increment at surface from SNF. The retrieved moisture field also exhibits a dryline at about x=290 km, a moisture tongue due to updraft and the troughs due to downdraft to the west and east (Fig. 7a). The strength of the updraft and downdraft as reflected by the isohume shapes is weaker than that from CNTL or 'nature'. Their locations near the ground are shifted eastwards relative to the 'truth'. The isohumes have shapes different from the 'truth' and are smoother than the 'true' isohumes (Fig. 7b). Overall, this analysis does not match the 'nature' as

well as the analysis of CNTL. The overall correlation coefficient of increment fields is reduced to 0.83.

Experiment CNTL has a flow-dependent background error covariance based on known background error while experiment SNF assumes an isotropic one. Their comparison illustrates the importance of accurate background error covariance. The problem is, however, that the background error covariance is never known exactly. In order to improve actual analysis in numerical weather prediction, it is necessary to seek feasible method to obtain the background error covariance as accurately as possible. Using an isotropic filter, we can obtain an analysis that is much closer to the 'truth' than the initial background field. As a result, the background error may be computed by subtracting the background from the isotropic analysis, which we call the updated (from that based on initial background) background error. Based on this consideration, experiment SUF is performed, which performs a second analysis starting from the same smoothed background but using an anisotropic filter based on the error field calculated as the difference between the output of SNF and the background. This analysis matches the 'truth' much better than that of SNF as shown in Fig. 8, even though the improvement is reflected clearly in the overall correlation coefficient (0.832 versus 0.830). The surface increment field (Fig. 8b) contains finer structures that are consistent with pattern of 'truth' increment field at the surface. In the vertical cross-section (Fig. 8a), the isohumes with specific humidity of 4, 6 and 8 g kg $^{-1}$ follow the 'truth' much better than those in Fig. 7a. The fine-scale moisture bulge near x = 290 km is also recovered well in this retrieval. Meanwhile, the maximum of 18.65 g kg⁻¹ is closer to the 'truth' value of 18.64 g kg⁻¹ than the 18.79 g kg⁻¹ from SNF.

The three experiments discussed above demonstrate that the 3DVAR system with flowdependent background error covariance realized through an anisotropic spatial filer provides better analysis than that with isotropic covariance. This is true even when the background error is estimated using a first-pass analysis that utilizes flow-independent error covariance.

c. Retrievals with vertically logarithmic background

The background in above three experiments comes from smoothing the 'truth'. This background, shown in Fig. 4, gives to some extent the physical structure of moisture at the larger scales and also contains information on the vertical moisture distribution. To understand how much the analysis system depends on the structure information present in the background, we conduct another two experiments in which the background is specified using a logarithmic function vertical profile. This profile decreases from a value of 12 g kg⁻¹ at the surface to zero at 17 km, the top of the analysis domain. This profile is used to specify the background q_v values on each terrain-following grid level, therefore, the background values are uniform along the model levels. Such a background supplies no realistic physical information on the structure of moisture, so that successful analysis has to extract structure information from the observations with the help of background error covariance. Two parallel experiments are performed. Experiment LNF uses the isotropic filter and experiment LTF uses anisotropic one that is based on the true error field. The vertical cross-sections of retrieved moisture field for these two experiments are presented in Fig. 9 and Fig. 10, respectively. As expected, the vertical structure of the analysis using flow-dependent background error is much better than that using isotropic one. For the former, the isohumes generally follow the 'true' isohumes except for near the boundaries. The dryline is reflected by the almost vertically oriented boundary between the dry and moist air in the lowest 1.5 km. But there are more errors near the boundaries in Fig. 9 (for experiment LTF) than in Fig. 5 (for experiment CNTL). This can be explained by the fact that, with the logarithmic background, the 3D moisture structure is mostly recovered from the GPS slant-path

water vapor observations but there are few slant-paths near the boundaries. For the retrieval of the isotropic filter case (Fig. 10), in addition to those problems near the boundaries, the dryline strength is weaker and the boundary separating the moist and dry air shows a significant slope at the low-levels. The structure is more symmetric in the east-west direction in accord with the isotropy and the moist bulge near x = 288 km is completely missed in this analysis.

As we have explained previously, the inclusion of the background term in the 3DVAR analysis eliminates the under-determinedness problem. So even with a background that is worse than the logarithmic one tested above, 3DVAR analysis is still feasible though the analysis is poorer. This is confirmed by an experiment that used a three-dimensionally homogeneous, i.e., a constant, background (results not shown). An analysis could not be obtained, i.e., the minimization procedure did not converge, when we removed the background term.

The above experiments show that our 3DVAR system is capable of recovering reasonably well the three-dimensional moisture structure from ground-based GPS slant-path water vapor and surface moisture observations even when using a rather artificial logarithmic background. When flow-dependent background error information is known and properly used, the analysis is better.

5. Sensitivity Experiments

In this section, sensitivity experiments are performed to test several factors that can affect the quality of moisture analysis.

a. Impact of surface moisture observations

Sensitivity experiment STFNSFC excludes surface observations while other settings are same as CNTL. This is to test the effect of surface moisture observations on the retrieval. The

results show that there are only slight differences between this experiment and CNTL for moisture distribution above 300 meters AGL, indicating that the retrieval without surface observations can still capture major features of the 3D moisture field. The overall correlation coefficient between the increment fields of retrieval and that of 'truth' is now 0.894, a slight reduction from the 0.926 of CNTL. Another experiment SNFNSFC is conducted with an isotropic filter and no surface observation as well. The results show that the vertical structure of the dryline still can be recovered but the strength is much weaker, compared to the retrieval with surface observation, e.g., from the corresponding experiment SNF that also uses an isotropic filter. The most outstanding difference occurs in the horizontal moisture structure. The increment fields at the surface from these two experiments, i. e., STFNSFC and SNFNSFC, are presented in the Fig. 11. When the covariance based on the true error field is used, as in STFNSFC, the pattern of the increment field, Fig. 11a, is good even though the extrema are only half as large. When the covariance matrix is isotropic and no surface observation is used, as in SNFNSFC, the surface increment field, shown in Fig. 11b, does not match the 'true' increment field in Fig. 6a and the extrema are weaker. Comparison of these analysis increments tells us that the surface information plays an important role for accurate analysis near ground, especially when the background error covariance information is unknown or not used.

Figure 12 plots the correlation coefficients between the retrieval and 'truth' increment fields against the vertical model level. It can be seen that the correlation coefficients with surface observations is larger than those without surface observation, especially at the lowest levels (below the 4th model level). From this, we conclude that better analysis of moisture field near the ground depends on two factors: accurate background error covariance and surface observations. The best retrieval is obtained when both are included while the worst is obtained when neither is.

The overall correlation coefficient between the increment fields of retrieval and 'nature' is 0.67 for SNFNSFC, about 0.26 less than that of CNTL. The large drop in accuracy is due to differences at the lowest levels where the surface observations have significant impact. This is so since it is the overlapping slant lines in three-dimensional space that provide information for 3D water vapor retrieval. Near the surface, very few slant paths go through the atmosphere due to the relatively high viewing angles of most satellites. The lowest elevation angle of slant paths in our experiments is about 15 degrees. The relatively small analysis domain also limits the lowest elevation angle of usable paths. The inaccuracy in the surface moisture analysis influences the analysis at high levels because the GPS system provides integrated observations.

b. Impact of vertical filtering

To determine the effect of vertical filtering, only the horizontal filter is used in the experiment STFNVF. All other parameter settings are same as in CNTL. Figure 13 shows the vertical profiles of correlation coefficients of specific humidity increment from CNTL and STFNVF. It is clear that CNTL gives a better analysis than STFNVF does. There is almost no difference at the surface owing to the use of surface observations but the correlation coefficient of STFNVF is significant lower between the 2nd and 5th level, with the difference being larger than 0.3 at the 2nd level. Still, the correlation coefficients from 3rd to 13th level are larger than or equal to 0.8 so that pattern of analysis increment remains good. The gradient of the analysis increment is, however, clearly weaker than that of 'truth' increment at the low levels (not shown). Figure 13 also shows a general improvement in the quality of analysis at the upper levels when vertical filtering is included. Therefore, the vertical filtering is very important for the moisture analysis near the surface. It is so because in the absence of vertical filtering, surface observation information cannot be spread upward to yield a positive impact on the boundary-

layer analysis and the GPS system cannot provide observation information for the lowest levels as very few slant paths go through these levels. In conclusion, the vertical filtering helps spread observation information in the vertical and improves the quality of analysis.

c. Sensitivity to observation error

One of the advantages of OSSE is that observation data can be error-free, but the sensitivity to observation errors should be examined for practical use. This is done in experiment STF_ER, in which errors are added to both surface and slant-path water vapor observations. The experiment is otherwise the same as CNTL. Pseudo-observations of surface specific humidity are with normally distributed errors with standard deviations of 5% and slant-path water vapor pseudo-observations with normally distributed errors with standard deviations of 7%, larger than the percentage error of surface observations since ground-based GPS receivers do not directly measure integrated water vapor, but rather integrated delay. Compared to the experiment CNTL, the relative weights of GPS SWV observations, regular surface moisture observations are decreased to 80 and 400 because those observations are imposed errors.

The analysis of STF_ER also matches the 'truth' well, as seen from the vertical slice at y = 234 km in Fig. 14. Only the 2 g kg⁻¹ isohume is prominently different from the CNTL result. The analyzed maximum is 19.49 g kg⁻¹, 0.75 g kg⁻¹ larger than the 'truth' maximum of 18.64 g kg⁻¹. The horizontal structure (not shown) also matches truth very well below 7 km where 95% water vapor concentrates. Therefore, the recovered 3D moisture field from this 3DVAR system is not very sensitive to random errors present in the surface and slant-path moisture observations although the overall correlation coefficient between the retrieval and 'truth' analysis increments decreases from 0.926 to 0.79. Still, all major structures of dryline are recovered well.

d. Observation density test

Finally, the sensitivity of 3D moisture analysis to ground-based GPS receiver density is examined. The GPS receiver density is halved in the following experiments. Thus, there is now one surface receiver station every 8 grid intervals, giving a receiver network resolution of 288 km. The horizontal length scale in physical space, i.e., L_r in Eqs. (5) and (6), and the corresponding cutoff radii are enlarged since their choices should be related to receiver network density. The length scale should be large enough to fill the gaps between receiver stations. Two parallel experiments are conducted. One experiment, SNF_LR, uses isotropic filter and L_r is given a length 5-grid interval while the experiment STF_LR uses an anisotropic filter and 6-grid interval scale length. They should be compared respectively with experiments CNTL and SNF.

Figure 15 presents retrieval result for STF_LR. Comparing the east-west vertical cross-section at y = 234 km in Fig. 15a with that of CNTL in Fig. 5, we can see that the difference in the quality of analysis is relatively small, indicating that the 3D moisture retrieval is not very sensitive to the observation density when the true background error is used to model the background error covariance. This conclusion is also supported by the surface increment field (Fig. 15b). The overall correlation coefficient is about 0.87 for STF_LR, 0.06 less than that of CNTL. When the background error covariance is given in an isotropic form (SNF_LR), the overall correlation coefficient decreases to 0.68 from the 0.83 of the corresponding high station density case (SNF). This reduction is much larger than that for flow-dependent background error cases (CNTL and STF_LR). This means that the retrieval is more sensitive to receiver station density when no good background error covariance is available or used.

6. Conclusions and future plan

A new 3DVAR-based retrieval method is developed for recovering three-dimensional water vapor structure of atmosphere from a GPS observation network. This network provides integrated water vapor along slant-paths between GPS satellites and ground-based receivers, together with direct moisture measurements at the receiver sites. The ARPS mesoscale model is used to produce a 'true' atmospheric moisture field, which is used to construct simulated GPS slant-path water vapor and surface observation data. This new method includes a background term in the 3DVAR cost function, which for one thing avoids the under-determinedness problem. A three-dimensional Gaussian spatial filter is used to model isotropic background error covariance. Further, a flow-dependent background error covariance is modeled by multiplying this Gaussian filter with an error field-related filter. Three-dimensional variational retrieval experiments are conducted with this new method for an IHOP dryline case. The results are summarized as follows:

- 1) This variational retrieval method with isotropic background error covariance can properly recover mesoscale three-dimensional moisture structure and capture major features of water vapor field simulated by the model from surface moisture and GPS slant-path SWV observation data.
- 2) The use of flow-dependent background error covariance further improve the analysis. Fine-scale moisture structure and strong specific humidity gradient can be accurately recovered to match the 'truth' of dryline. Near the lateral boundaries and at the low levels, where few slant paths exist or overlap, the role of flow-dependent covariance is enhanced. Consequently, the retrieval in the boundary layer would be improved if more low-elevation angle slant paths were available.

- 3) Retrieval is still feasible with artificial logarithmic background even though the quality of analysis deteriorates; especially near the boundaries where few slant lines overlap.
- 4) Sensitivity experiments indicate that surface moisture observations are important for accurate analysis of water vapor field at low levels, and more so when no good information on background error covariance is available or used. The vertical component of the spatial filter is shown to be very beneficial, especially in data-sparse regions such as the model levels right above the ground; its main effect is the upward spread of surface moisture information.
- 5) Observation error sensitivity tests show that our analysis system is not very sensitive to errors in the surface moisture and SWV observations. Major dryline structures can still be recovered when normally distributed errors with standard deviations of 5 and 7%, respectively, are imposed on surface moisture and SWV observations. After halving ground-based receiver station density, dryline structure can be reasonably recovered when flow-dependent background error covariance is used. But the lower observation resolution worsens the boundary problem, leading to obvious decrease in the retrieval accuracy near lateral boundary and surface. The decrease is more when isotropic spatial filter is used.

In our analysis system, a Gaussian spatial filter is used to model the background error covariance as well as to save computational memory (as compared to storing the full **B** matrix). This treatment cannot guarantee the positive definite property of the modified covariance. Meanwhile, the larger is cutoff radii, the more expensive the algorithm becomes. One alternative is the recursive filter, which can be applied to achieve isotropic as well as anisotropic covariance (Wu et al. 2002; Purser et al. 2003a; b), although the realization of the latter with recursive filter is much more complicated. We plan to experiment with recursive filters due to their computational efficiency. In addition, we will use the retrieved moisture field to initialize a

mesoscale model and examine the impact of assimilating GPS SWV data on short-range precipitation forecast for the current dryline and other cases. Real GPS SWV data collected during the IHOP_2002 field experiment will also be tested.

Acknowledgement

This work was supported by NSF grant ATM0129892. Ming Xue was also supported by NSF ATM-9909007, ATM-0331594, EEC-0313747, DOT-FAA grant NA17RJ1227 and a grant from Chinese Natural Science Foundation No. 40028504. Drs. Keith Brewster, Jidong Gao, and Bill Martin are thanked for helpful discussions. The authors also benefited from exchanges with Drs. Randolph Ware and Yuanfu Xie.

References

- Bengtsson, L., G. Robinson, R. Anthes, K. Aonashi, A. Dodson, G. Elgered, G. Gendt, R.
 Gurney, M. Jietai, C. Mitchell, M. Mlaki, A. Rhodin, P. Silvestrin, R. Ware, R. Watson, and W. Wergen, 2003: The Use of GPS Measurements for Water Vapor Determination.
 Bull. of Amer. Meteor. Soc., 84, 1249-1258.
- Bevis, M., S. Businger, T. A. Herring, R. A. Anthes, C. Rocken, R. H. Ware, and S. Chiswell, 1994: GPS meteorology: Mapping zenith wet delays onto precipitable water. *J. Appl. Meteor.*, **33**, 379-386.
- Braun, J., C. Rocken, and R. Ware, 2001: Validation of line-of-sight water vapor measurements with GPS. *Radio Sci.*, **36**, 459-472.
- Brewster, K., 1996: Application of a Bratseth analysis scheme including Doppler radar data.

 *Preprints, 15th Conf. Wea. Anal. Forecasting, Norfolk, VA, Amer. Meteor. Soc., 92-95.
- Businger, S., S. R. Chiswell, M. Bevis, J. Duan, R. A. Anthes, C. Rocken, R. H. Ware, M. Exner, T. VanHove, and F. S. Solheim, 1996: The Promise of GPS in Atmospheric Monitoring. *Bull. of Amer. Meteor. Soc.*, 77, 5-18.
- Cucurull, L., F. Vandenberghe, D. Barker, E. Vilaclara, and A. Rius, 2004: Three-Dimensional Variational Data Assimilation of Ground-Based GPS ZTD and Meteorological Observations during the 14 December 2001 Storm Event over the Western Mediterranean Sea. *Mon. Wea. Rev.*, **132**, 749-763.
- Daley, R., 1991: Atmospheric Data Analysis. Cambridge University Press, 457 pp.
- de Pondeca, M. S. F. V. and X. Zou, 2001a: Moisture retrievals from simulated zenith delay "observations" and their impact on short-range precipitation forecasts. *Tellus*, **53**, 192.

- —, 2001b: A Case Study of the Variational Assimilation of GPS Zenith Delay Observations into a Mesoscale Model. *J. Appl. Meteor.*, **40**, 1559-1576.
- Duan, J., M. Bevis, P. Fang, Y. Bock, S. Chiswell, S. Businger, C. Rocken, F. Solheim, T. van Hove, R. Ware, S. McClusky, T. A. Herring, and R. W. King, 1996: GPS Meteorology:

 Direct Estimation of the Absolute Value of Precipitable Water. *J. Appl. Meteor.*, **35**, 830-838.
- Duchon, C. E., 1979: Lanczos filtering in one and two dimensions. *J. Appl. Meteor.*, **18**, 1016-1022.
- Emanuel, K., D. Raymond, A. Betts, L. Bosart, C. Bretherton, K. Droegemeier, B. Farrell, J. M. Fritsch, R. Houze, M. LeMone, D. Lilly, R. Rotunno, M. Shapiro, R. Smith, and T. A, 1995: Report of the first Prospectus Development Team of the U.S. Weather Research Program to NOAA and the NSF. *Bull. Amer. Meteor. Soc.*, **76**, 1194-1208.
- Falvey, M. and J. Beavan, 2002: The Impact of GPS Precipitable Water Assimilation on Mesoscale Model Retrievals of Orographic Rainfall during SALPEX'96{ast}. *Mon. Wea. Rev.*, **130**, 2874-2888.
- Guo, Y.-R., Y.-H. Kuo, J. Dudhia, D. Parsons, and C. Rocken, 2000: Four-dimensional variational data assimilation of heterogeneous mesoscale observations for a strong convective case. *Mon. Wea. Rev.*, **128**, 619-643.
- Ha, S.-Y., Y.-H. Kuo, Y.-R. Guo, and G.-H. Lim, 2003: Variational Assimilation of Slant-Path Wet Delay Measurements from a Hypothetical Ground-Based GPS Network. Part I: Comparison with Precipitable Water Assimilation. *Mon. Wea. Rev.*, **131**, 2635-2655.
- Hayden, C. M. and J. Purser, 1995: Recursive filter objective analysis of meteorological fields: Applications to NESDIS operational processing. *J. Appl. Meteor.*, **34**, 3-15.

- Huang, X.-Y., 2000: Variational analysis using spatial filters. Mon. Wea. Rev., 128, 2588–2600.
- Kuo, Y.-H., Y.-R. Guo, and E. R. Westerwater, 1993: Assimilation of precipitable water measurements into a mesoscale numerical model. *Mon. Wea. Rev.*, **121**, 1215-1238.
- Kuo, Y.-H., X. Zou, and Y. R. Guo, 1996: Variational assimilation of precipitable water using a nonhydrostatic mesoscale adjoint model. Part I: Moisture retrieval and sensitivity experiments. *Mon. Wea. Rev.*, **124**, 122-147.
- Lorenc, A. C., 1981: A global three-dimensional multivariate statistical interpolation scheme. *Mon. Wea. Rev.*, **109**, 701-721.
- MacDonald, A. E., Y. Xie, and R. H. Ware, 2002: Diagnosis of Three-Dimensional Water Vapor Using a GPS Network. *Mon. Wea. Rev.*, **130**, 386-397.
- Purser, R. J., W.-S. Wu, D. F. Parrish, and N. M. Roberts, 2003a: Numerical Aspects of the Application of Recursive Filters to Variational Statistical Analysis. Part II: Spatially Inhomogeneous and Anisotropic General Covariances. *Mon. Wea. Rev.*, **131**, 1536-1548.
- —, 2003b: Numerical Aspects of the Application of Recursive Filters to Variational Statistical Analysis. Part I: Spatially Homogeneous and Isotropic Gaussian Covariances. *Mon. Wea. Rev.*, **131**, 1524-1535.
- Riishojgaard, L. P., 1998: A direct way of specifying flow-dependent background error correlations for meteorological analysis systems. *Tellus*, **50A**, 42-57.
- Ware, R., C. Alber, C. Rocken, and F. Solheim, 1997: Sensing integrated water vapor along GPS ray paths. *Geophys. Res. Lett.*, **24**, 417–420.
- Ware, R. H., D. W. Fulker, S. A. Stein, D. N. Anderson, S. K. Avery, R. D. Clark, K. K. Droegemeier, J. P. Kuettner, J. B. Minster, and S. Sorooshian, 2000: SuomiNet: A Real-

- Time National GPS Network for Atmospheric Research and Education. *Bull. of Amer. Meteor. Soc.*, **81**, 677-694.
- Wolfe, D. E. and S. I. Gutman, 2000: Developing an Operational, Surface-Based, GPS, Water Vapor Observing System for NOAA: Network Design and Results. *J. Atmos. Oceanic Tech.*, **17**, 426-440.
- Wu, W.-S., R. J. Purser, and D. F. Parrish, 2002: Three-Dimensional Variational Analysis with Spatially Inhomogeneous Covariances. *Mon. Wea. Rev.*, **130**, 2905-2916.
- Xue, M., K. K. Droegemeier, and V. Wong, 2000: The Advanced Regional Prediction System
 (ARPS) A multiscale nonhydrostatic atmospheric simulation and prediction tool. Part I:
 Model dynamics and verification. *Meteor. Atmos. Physics*, 75, 161-193.
- Xue, M., K. Brewster, D. Weber, K. W. Thomas, F. Kong, and E. Kemp, 2002: Realtime storm-scale forecast support for IHOP 2002 at CAPS. *Preprint, 15th Conf. Num. Wea. Pred.*and 19th Conf. Wea. Aanl. Forecasting, San Antonio, TX, Amer. Meteor. Soc., 124-126.

List of Table

Table 1. List of moisture retrieval experiments

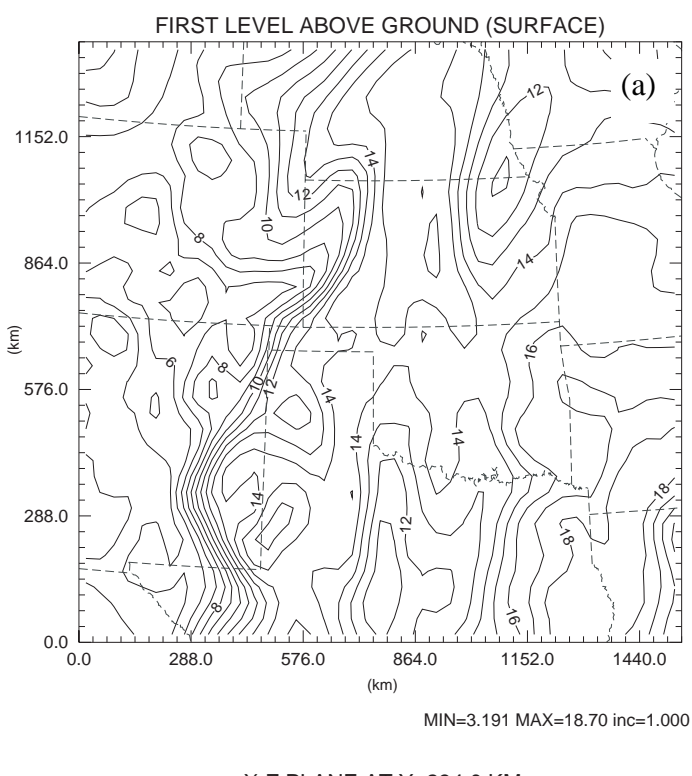
Table 1. List of moisture retrieval experiments

Experiment	background	Flow-dependent B	Obs, obs error	Obs resolution	Filter	
						coefficient
CNTL	smoothed truth	Yes, on true background	SWV+sfc, no	1 ob/4 grid	3D	0.926
		error		intervals		
SNF	smoothed truth	No	SWV+sfc, no	1 ob/4 grid	3D	0.830
				intervals		
SUF	smoothed truth	Yes, on updated background	SWV+sfc, no	1 ob/4 grid	3D	0.832
				intervals		
LTF	Logarithmic	Yes, on true background	SWV+sfc, no	1 ob/4 grid	3D	0.827
	-	error		intervals		
LNF	logarithmic	No	SWV+sfc, no	1 ob/4 grid	3D	0.821
				intervals		
STFNSFC	smoothed truth	Yes, on true background	SWV, no	1 ob/4 grid	3D	0.894
		error		intervals		
SNFNSFC	smoothed truth	No	SWV, no	1 ob/4 grid	3D	0.668
				intervals		
STFNVF	smoothed truth	Yes, on true background	SWV+sfc, no	1 ob/4 grid	2D	0.801
		error		intervals		
STF_ER	smoothed truth	Yes, on true background	SWV+sfc, yes	1 ob/4 grid	3D	0.790
		error	•	intervals		
SNF_LR	smoothed truth	No	SWV+sfc, no	1 ob/8 grid	3D	0.679
				intervals		
STF_LR	smoothed truth	Yes, on true background	SWV+sfc, no	1 ob/8 grid	3D	0.870
		error		intervals		

List of Figures

- Figure 1. Specific humidity field (g kg⁻¹) from the ARPS simulated 'nature' for an IHOP case at 20 UTC, 19 June, 2002 (a) at the surface and (b) in the east-west vertical cross-section at y = 234 km. A roughly north-south zone of strong horizontal moisture gradient is located to the west of Kansas, Oklahoma and Texas, representing the dryline. In vertical cross-section, a boundary between the dry and moist air is oriented nearly vertically in the lowest 1.5 km then turns horizontal to the east.
- Figure 2. A schematic of hypothetic ground-based GPS observation network whose data are analyzed using 3DVAR. Shaded surface represents terrain. Dark solid lines are slant paths between ground-based GPS receivers and GPS satellites. Dotted lines give a sense of the vertically stretched grid although the actual grid levels are in terrain-following coordinate.
- Figure 3. Specific humidity increment field in g kg⁻¹ at the surface from single moisture observation tests, (a) for 3DVAR analysis with flow-dependent background error covariance and (b) for 3DVAR analysis with isotropic covariance. Only one specific humidity observation is present whose location is marked by the black dot in the figure.
- Figure 4. Background specific humidity field in g kg⁻¹, obtained by smoothing 'nature' 50 times using a 9-point filter in the horizontal, (a) at the surface and (b) in the east-west vertical cross-section at y = 234 km.
- Figure 5. East-west vertical cross-section of specific humidity field (g kg^{-1}) at y = 234 km. Solid line is for 'nature' and dotted line from CNTL.
- Figure 6. Specific humidity increment field in g kg⁻¹ at the surface (a) from 'nature' and (b) from CNTL. Dashed lines represent negative values and solid lines positive values.

- Figure 7. (a) East-west vertical cross-section of specific humidity field (g kg $^{-1}$) at y = 234 km where solid lines are for 'nature' and dotted lines for experiment SNF. (b) Analysis increment of specific humidity (g kg $^{-1}$) at the surface from experiment SNF, where dashed lines are for negative values and solid line for positive values.
- Figure 8. As Fig. 7 but for experiment SUF.
- Figure 9. As Fig. 5 but dotted lines are from experiment LTF.
- Figure 10. As Fig. 5 but dotted lines are from experiment LNF.
- Figure 11. As Fig. 6 but (a) is for experiment STFNSFC SNFNSFC (b) is for experiment SNFNSFCSTFNSFC.
- Figure 12. Profiles of correlation coefficient of specific humidity increment (difference from background, in g kg⁻¹) between those of 'nature' and 3DVAR analysis from experiments CNTL, STFNSFC, SNFNSFC, and SNF, plotted for different model levels. Mean heights of model levels are listed as follows (in km): 0.80, 0.89, 0.98, 1.12, 1.29, 1.50, 1.73, 2.00, 2.28, 2.58, 2.90, 3.24, 3.58, 3.94, 4.30, 4.66, 5.04, 5.41, 5.79, 6.16, 6.54, 6.92, 7.30, 7.67, 8.05, 8.43, 8.81, 9.20, 9.59, 9.98, 10.38, 10.79, 11.21, 11.65, 12.10, 12.57, 13.07, 13.59, 14.14, 14.72, 15.34, 16.00, 16.66.
- Figure 13. Profiles of correlation coefficient of specific humidity increment (g kg⁻¹) between those of 'nature' and 3DVAR analysis from CNTL (solid line) and experiment STFNZF (dotted line).
- Figure 14. As Fig. 5 but dotted lines are for experiment STF_ER.
- Figure 15. As Fig. 7 but for experiment STF_LR.



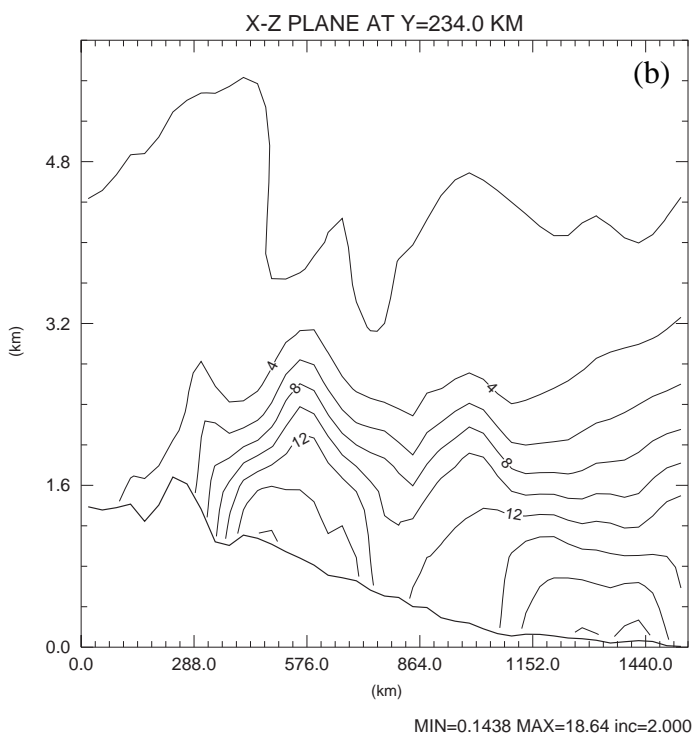


Figure 1. Specific humidity field (g kg $^{-1}$) from the ARPS simulated 'nature' for an IHOP case at 20 UTC, 19 June, 2002 (a) at the surface and (b) in the east-west vertical cross-section at y = 234 km. A roughly north-south zone of strong horizontal moisture gradient is located to the west of Kansas, Oklahoma and Texas, representing the dryline. In vertical cross-section, a boundary between the dry and moist air is oriented nearly vertically in the lowest 1.5 km then turns horizontal to the east.

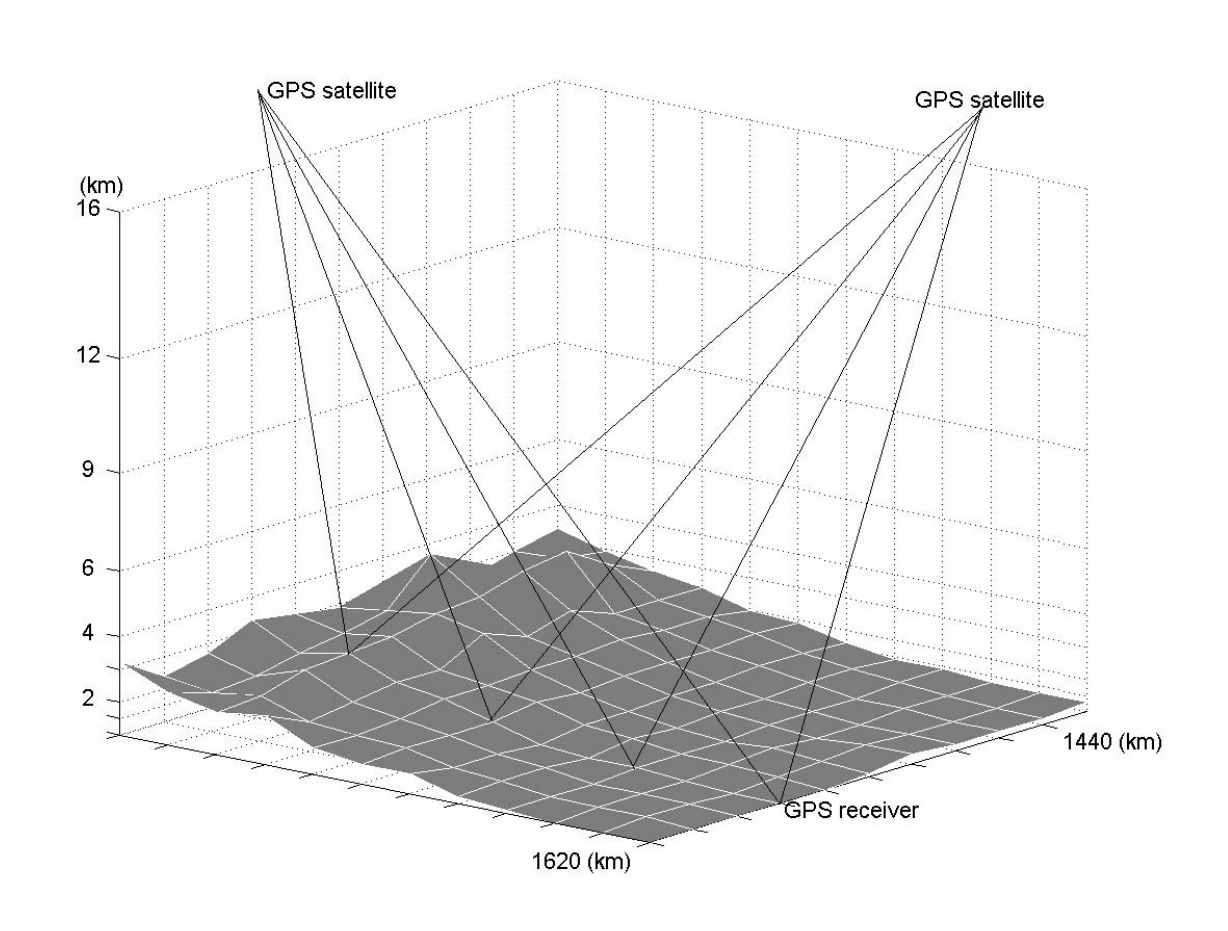


Figure 2. A schematic of hypothetic ground-based GPS observation network whose data are analyzed using 3DVAR. Shaded surface represents terrain. Dark solid lines are slant paths between ground-based GPS receivers and GPS satellites. Dotted lines give a sense of the vertically stretched grid although the actual grid levels are in terrain-following coordinate.

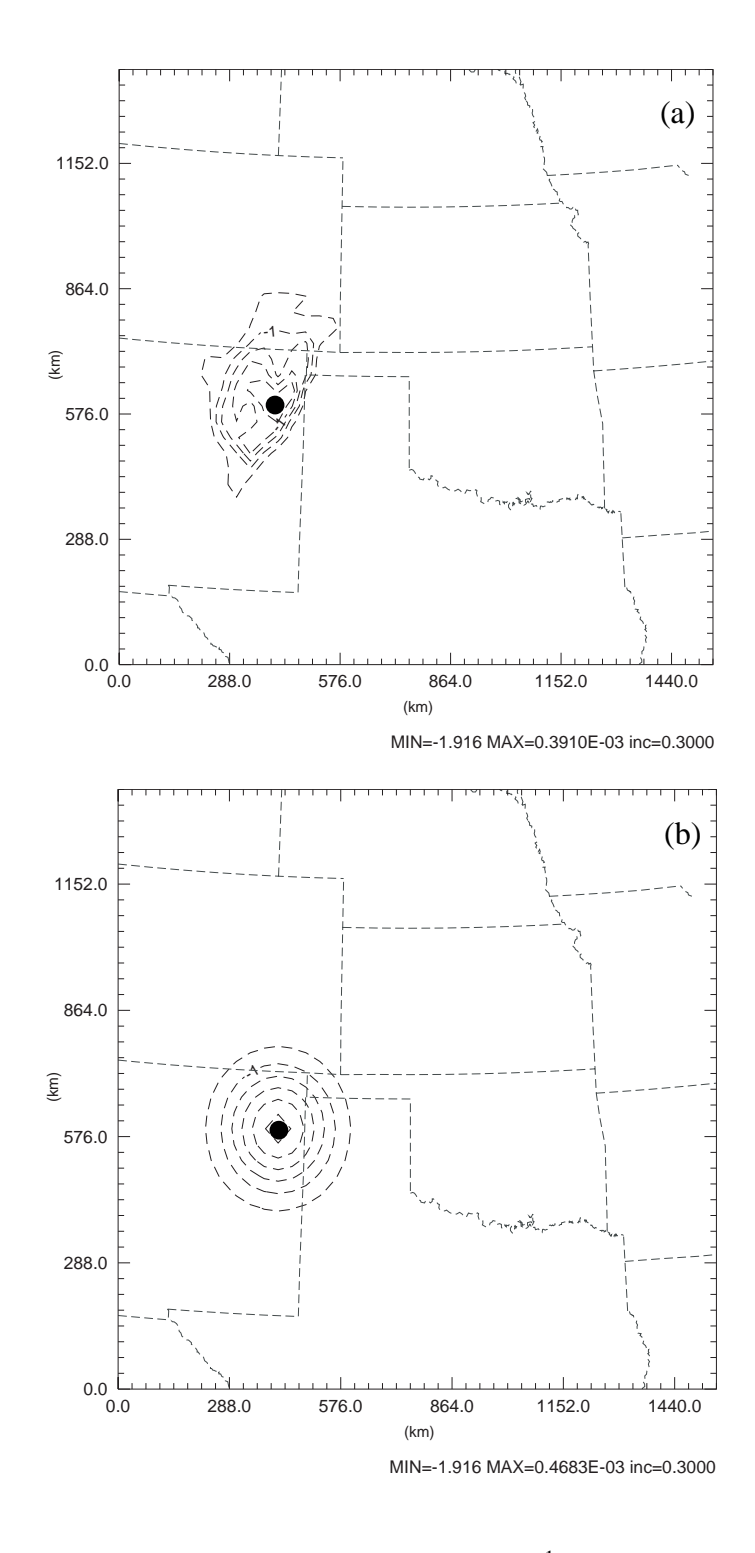


Figure 3. Specific humidity increment field in g kg⁻¹ at the surface from single moisture observation tests, (a) for 3DVAR analysis with flow-dependent background error covariance and (b) for 3DVAR analysis with isotropic covariance. Only one specific humidity observation is present whose location is marked by the black dot in the figure.

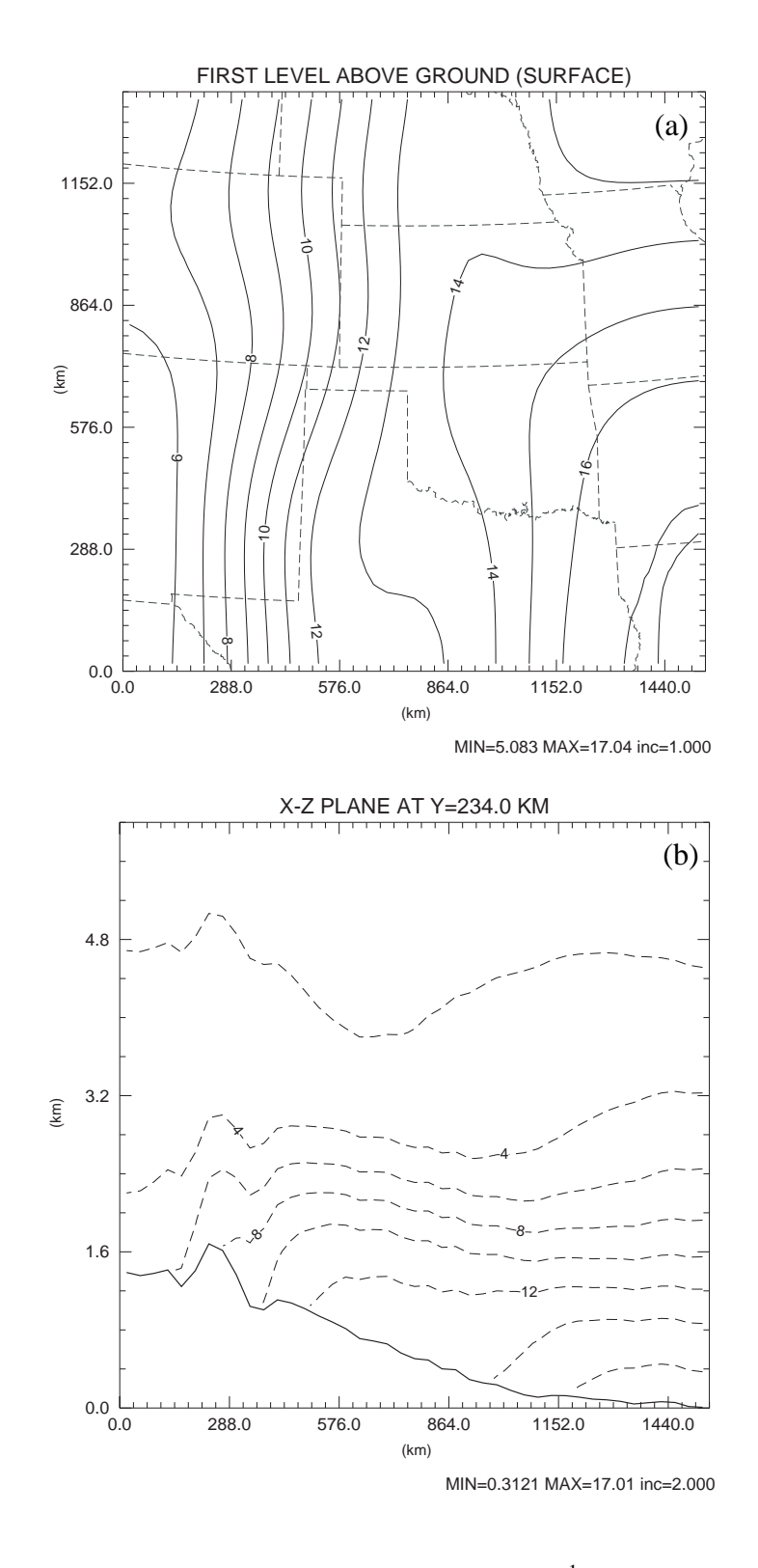


Figure 4. Background specific humidity field in g kg^{-1} , obtained by smoothing 'nature' 50 times using a 9-point filter in the horizontal, (a) at the surface and (b) in the east-west vertical cross-section at y = 234 km.

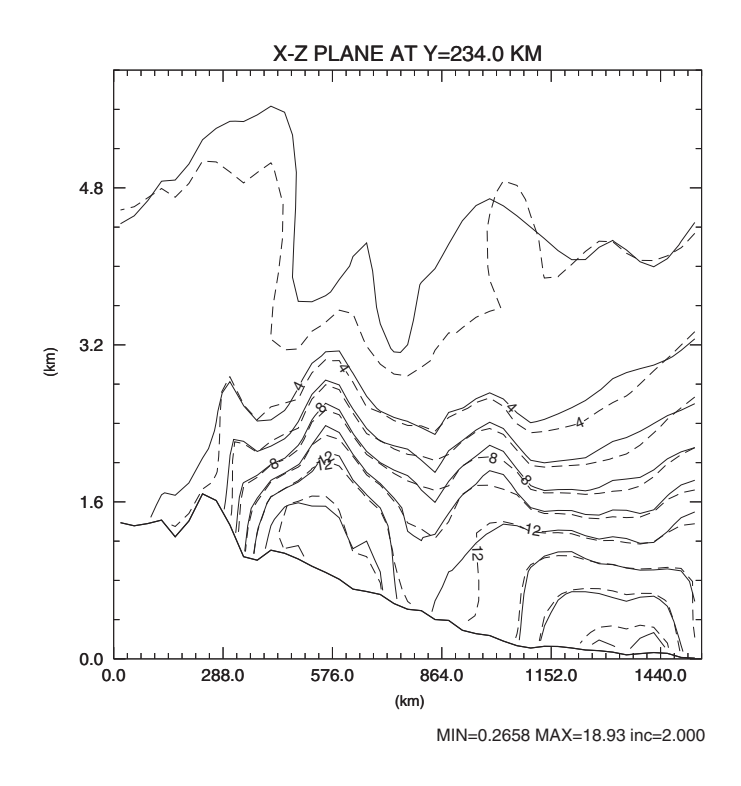
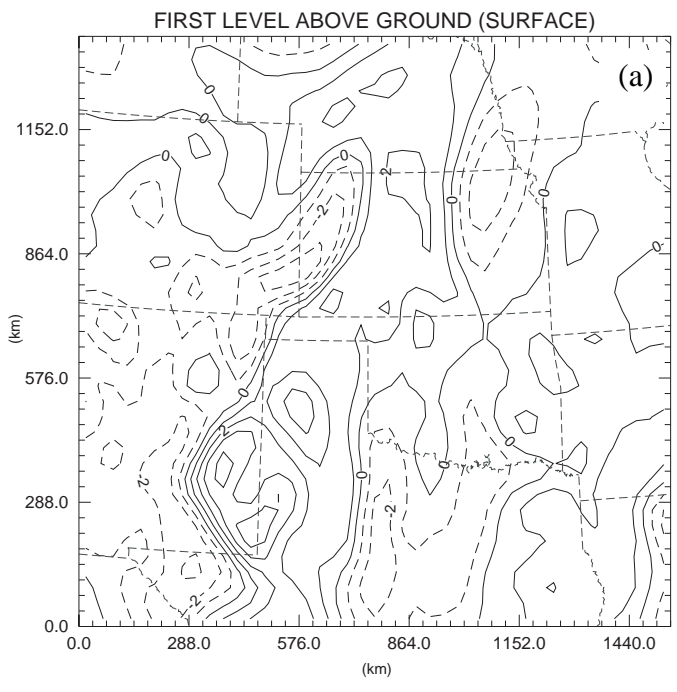
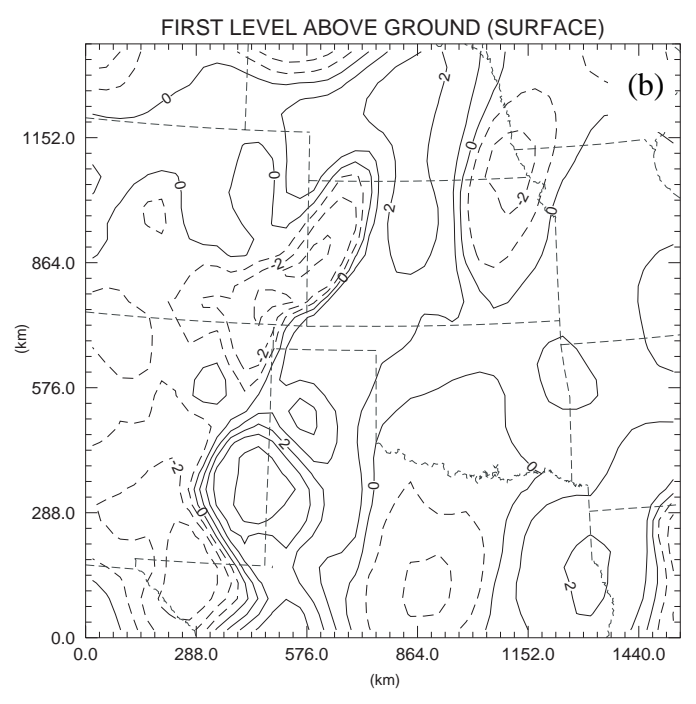


Figure 5. East-west vertical cross-section of specific humidity field (g kg^{-1}) at y = 234 km. Solid line is for 'nature' and dotted line from CNTL.



MIN=-3.789 MAX=4.649 inc=1.000



MIN=-3.790 MAX=4.839 inc=1.000

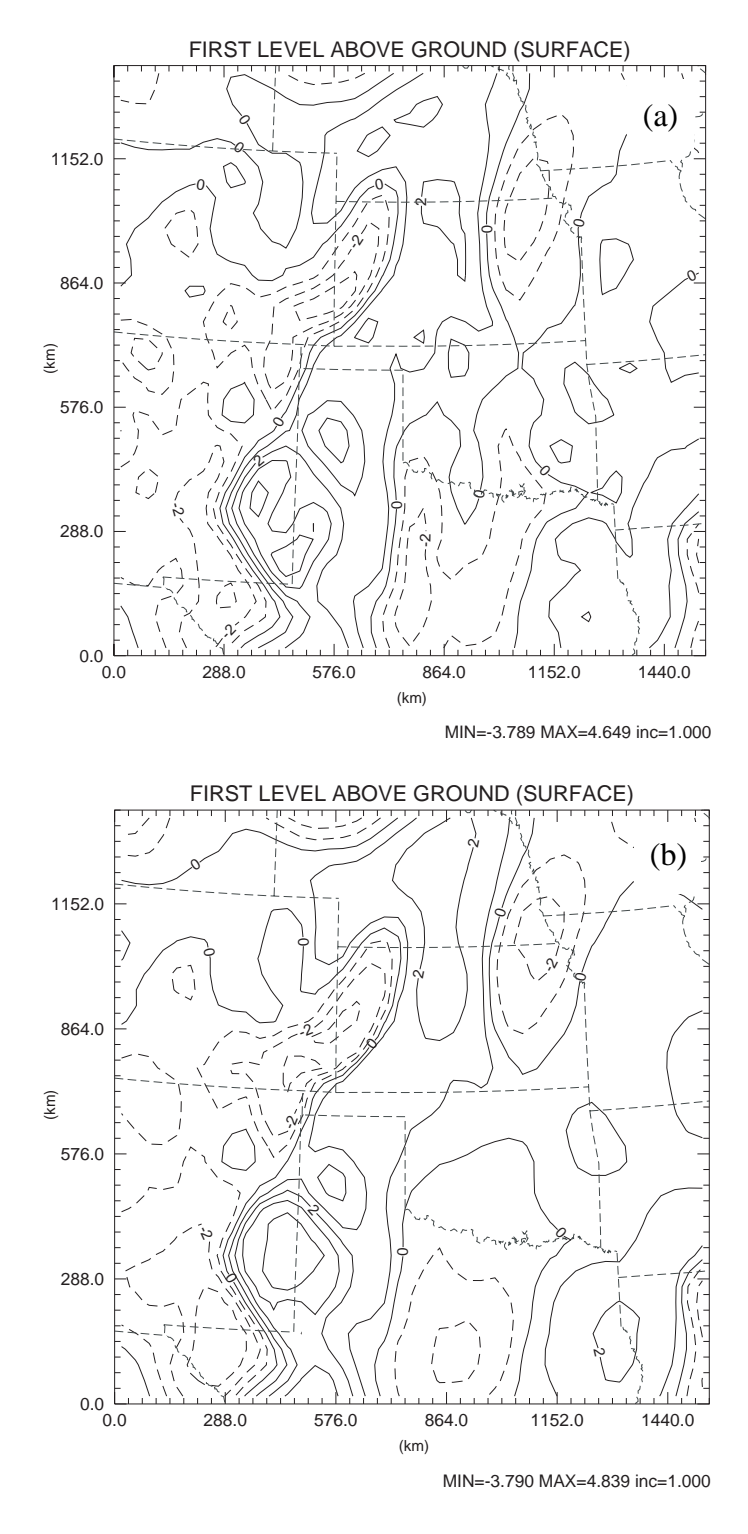
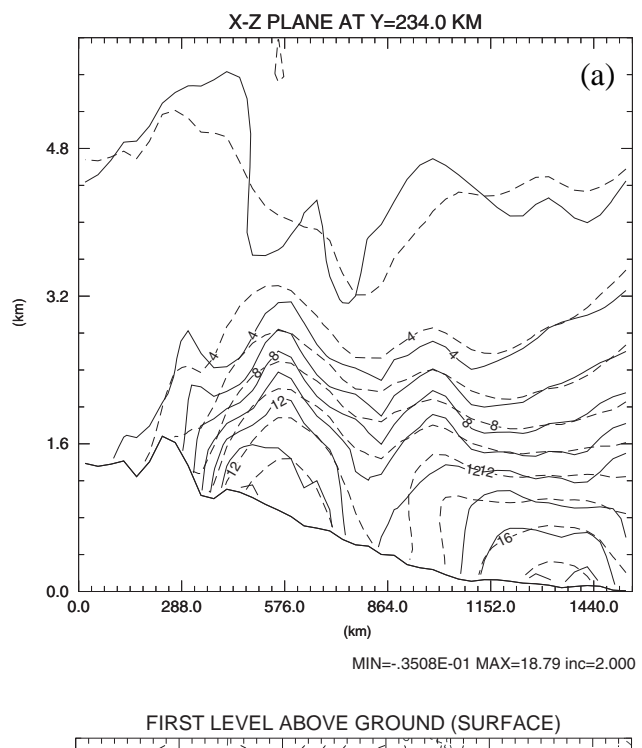


Figure 6. Specific humidity increment field in g kg⁻¹ at the surface (a) from 'nature' and (b) from CNTL. Dashed lines represent negative values and solid lines positive values.



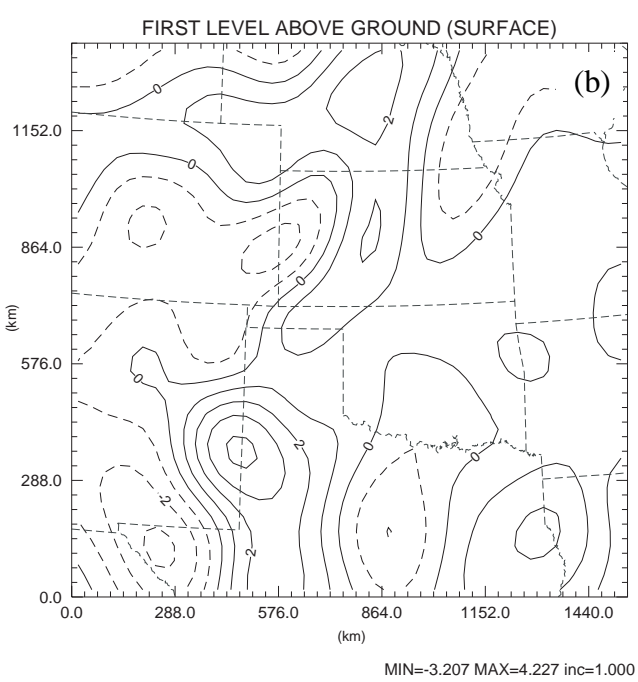
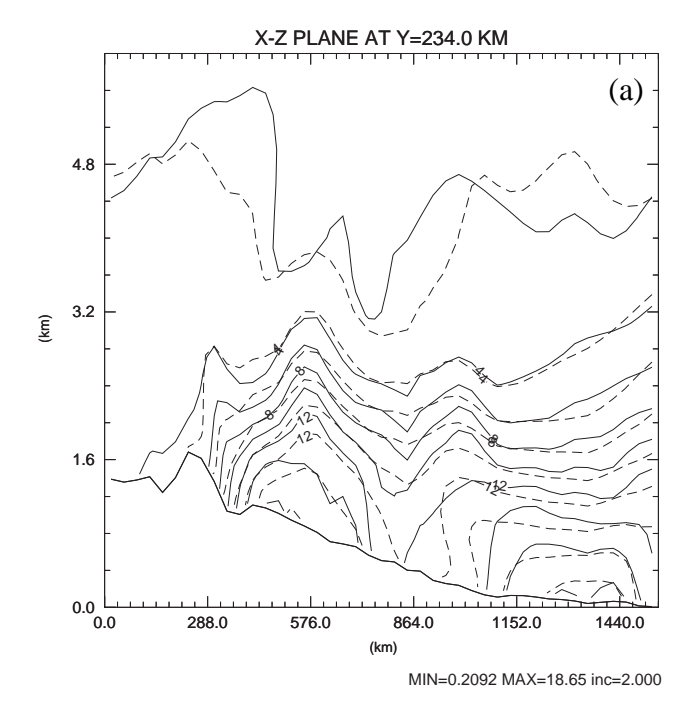
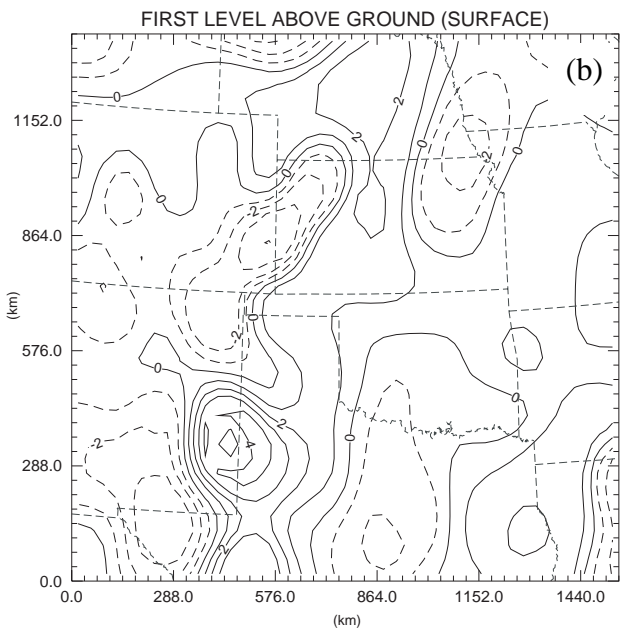


Figure 7. (a) East-west vertical cross-section of specific humidity field (g kg $^{-1}$) at y = 234 km where solid lines are for 'nature' and dotted lines for experiment SNF. (b) Analysis increment of specific humidity (g kg $^{-1}$) at the surface from experiment SNF, where dashed lines are for negative values and solid line for positive values.





MIN=-3.731 MAX=4.589 inc=1.000

Figure 8. As Fig. 7 but for experiment SUF.

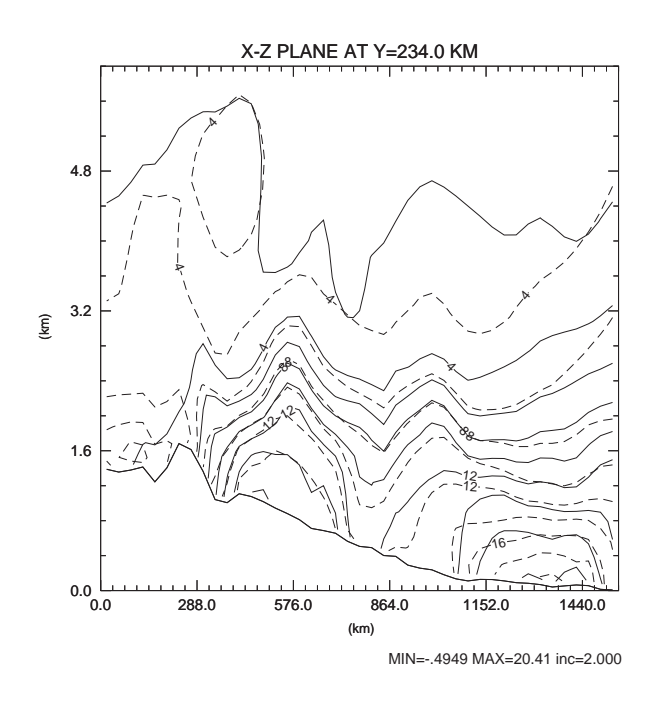


Figure 9. As Fig. 5 but dotted lines are from experiment LTF.

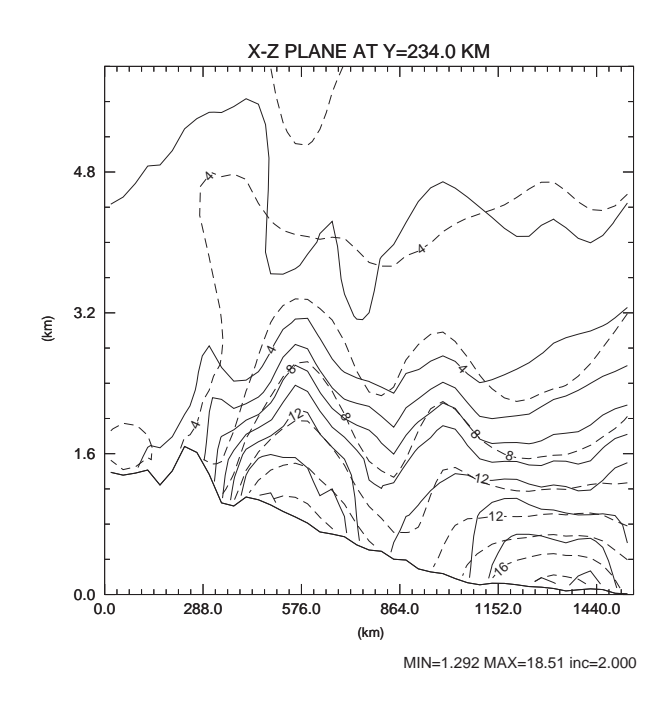
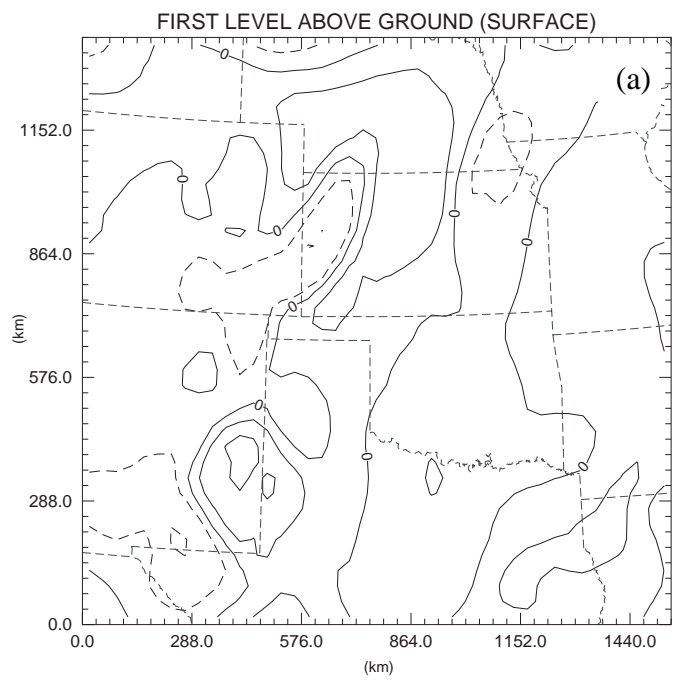
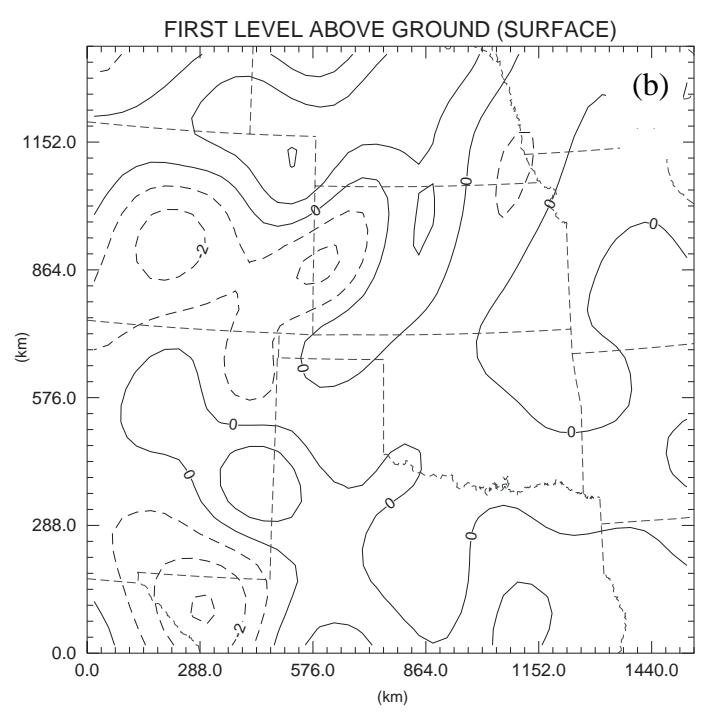


Figure 10. As Fig. 5 but dotted lines are from experiment LNF.



MIN=-2.039 MAX=2.419 inc=1.000



MIN=-3.119 MAX=2.028 inc=1.000

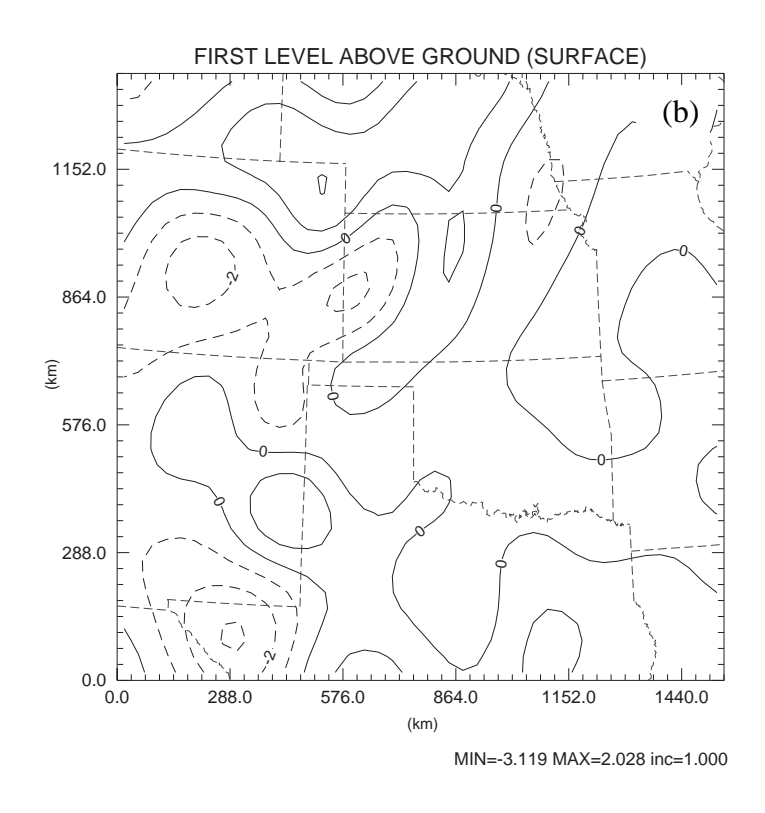


Figure 11. As Fig. 6 but (a) is for experiment STFNSFC (b) is for experiment SNFNSFC.

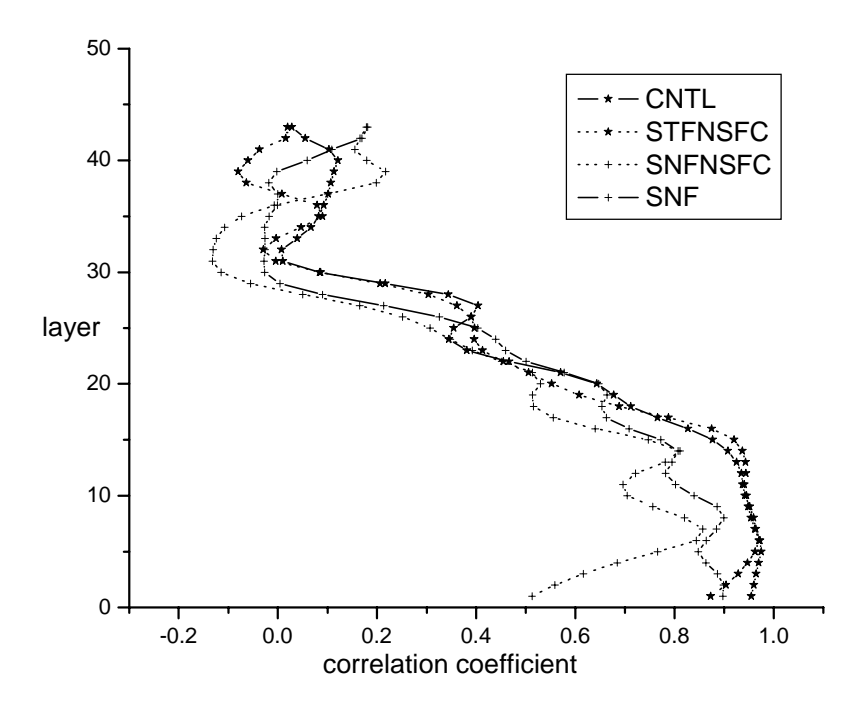


Figure 12. Profiles of correlation coefficient of specific humidity increment (difference from background, in g kg⁻¹) between those of 'nature' and 3DVAR analysis from experiments CNTL, STFNSFC, SNFNSFC, and SNF, plotted for different model levels. Mean heights of model levels are listed as follows (in km): 0.80, 0.89, 0.98, 1.12, 1.29, 1.50, 1.73, 2.00, 2.28, 2.58, 2.90, 3.24, 3.58, 3.94, 4.30, 4.66, 5.04, 5.41, 5.79, 6.16, 6.54, 6.92, 7.30, 7.67, 8.05, 8.43, 8.81, 9.20, 9.59, 9.98, 10.38, 10.79, 11.21, 11.65, 12.10, 12.57, 13.07, 13.59, 14.14, 14.72, 15.34, 16.00, 16.66.

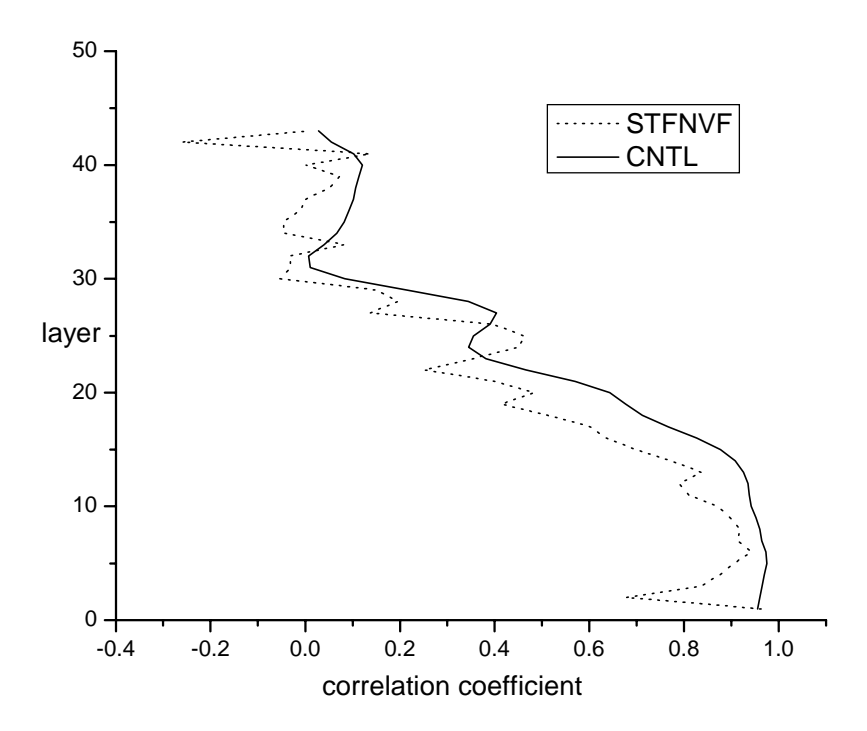


Figure 13. Profiles of correlation coefficient of specific humidity increment (g kg⁻¹) between those of 'nature' and 3DVAR analysis from CNTL (solid line) and experiment STFNVF (dotted line). Mean height of each level is given in the caption of Figure 12.

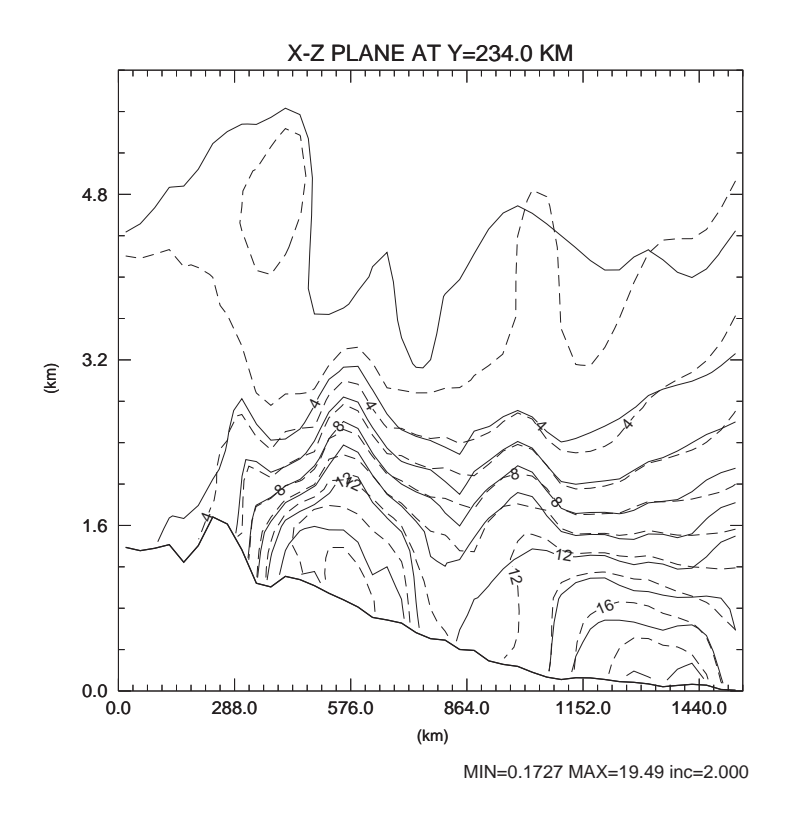
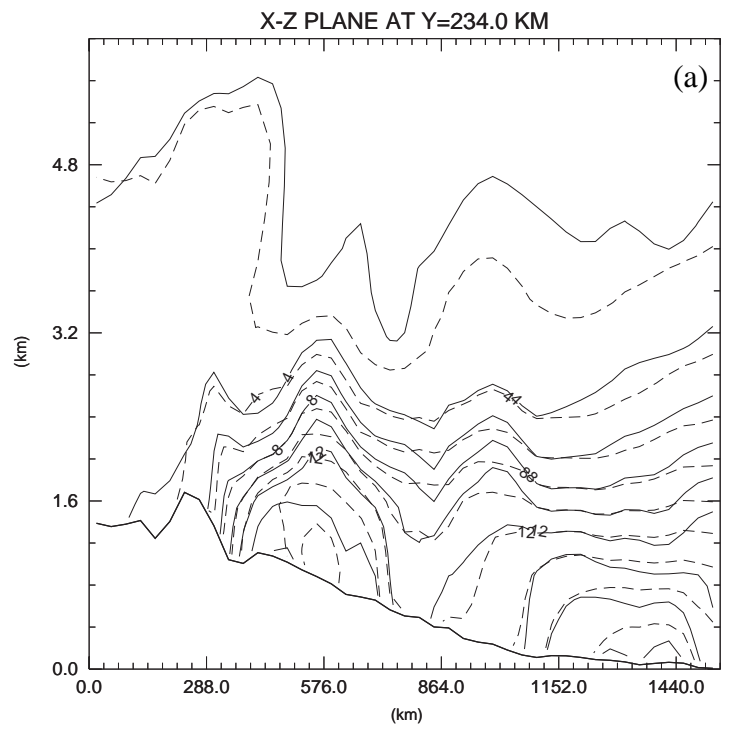


Figure 14. As Fig. 5 but dotted lines are for experiment STF_ER.



MIN=0.1097 MAX=19.05 inc=2.000

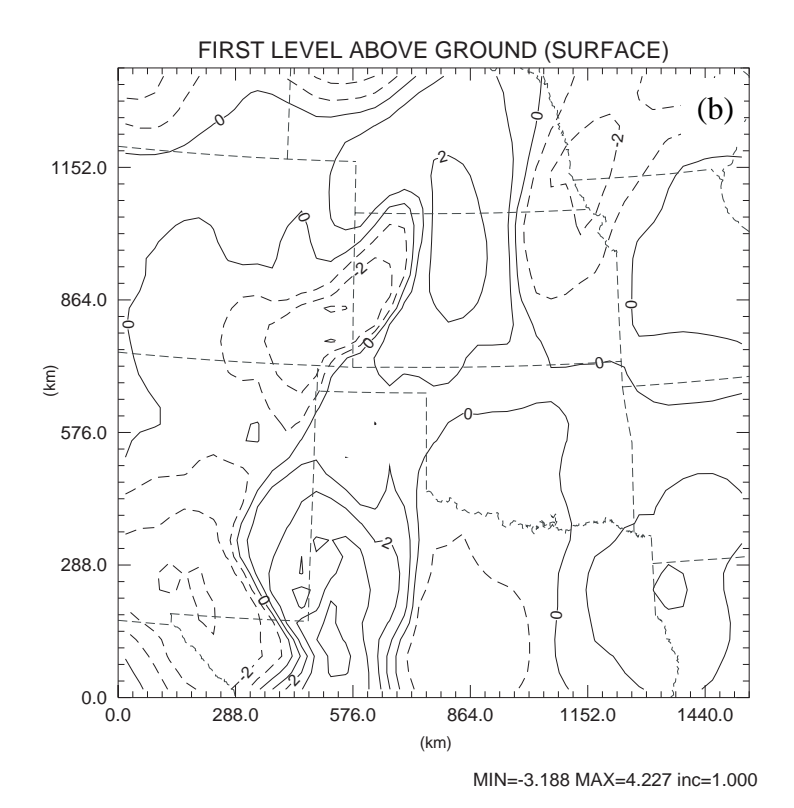


Figure 15. As Fig. 7 but for experiment STF_LR.